A Unified Framework for Interface Conformability Optimisation: Stress, Spectral, and Topological Constraints

Swapan Samanta

Independent Researcher, Indoriv Clinical Research Centre, Kolkata, West Bengal, India

DOI: https://doi.org/10.51244/IJRSI.2026.1305000293

Received: 11 May 2026; Accepted: 16 May 2026; Published: 17 June 2026

ABSTRACT

We develop a mathematical framework for optimising interfaces between discrete rigid elements and continuous irregular substrates. While contact mechanics analyses stress for given geometries and homogenisation theory treats continuous–discrete transitions, the inverse problem—determining optimal element size from substrate topology and material constraints—has lacked systematic treatment. We introduce three independent dimensionless metrics: a stress-based Conformability Index (CI), a spectral Critical Wavelength Ratio (CWR), and a topology-inspired Topological Obstruction Number (TON). Through variational energy minimisation, we show these metrics emerge naturally from a unified principle rather than being ad hoc constructs. An independent derivation via quantisation theory recovers identical scaling exponents, providing internal consistency without empirical data. We derive universal scaling laws—d ∝ t, d ∝ σz^(−1/(H+1)), d ∝ √(σy/E)—with parameter-independent exponents offering falsifiable predictions. Ceramic tile installation serves as the canonical example, while the mathematical structure applies wherever rigid discrete coverings interface continuous irregular fields under structural constraints.

Keywords: interface conformability, discrete–continuous optimisation, contact mechanics, spectral analysis, variational methods, scaling laws, interface mechanics

Scope and Limitations

This paper establishes a theoretical framework for interface conformability optimisation within a defined regime: linear elastic thin plates on rigid substrates under quasi-static loading. We derive three complementary metrics, demonstrate their independence, and extract universal scaling laws with testable exponents. The framework explicitly identifies its boundaries—compliant substrates, dynamic loading, large deformations, and adhesive-dominated interfaces lie outside the current scope and require extensions. Empirical validation is deferred to future experimental work; the present contribution is the mathematical structure, its internal consistency, and the specification of falsification criteria. Threshold values (CI < 0.35, TON < 3) are provisional and require calibration. We claim identification of a previously unformalised optimisation class and a minimal theoretical basis for it—not a comprehensive engineering solution.

Statement of Novelty

The principal novelty lies not in any individual metric—stress analysis, spectral methods, and critical point theory each have established precedents—but in four specific contributions: (1) formulation of the inverse conformability problem as a distinct optimisation class; (2) demonstration that three functionally independent constraints (stress, spectral, topological) are each necessary and jointly insufficient to be reduced, meaning no proper subset predicts all failure modes; (3) derivation of parameter-independent scaling exponents from variational mechanics, independently recovered through quantisation theory; and (4) construction of explicit falsification criteria enabling sharp empirical tests. We demonstrate through benchmark cases that Hertz contact mechanics, Persson spectral theory, and classical plate theory each fail individually where the integrated framework succeeds.

ISSN No. 2321-2705 | DOI: 10.51244/IJRSI |Volume XIII Issue V May 2026

INTRODUCTION

Consider a rigid plate resting on an irregular substrate. If the plate is large relative to the substrate's surface features, it bridges across voids, concentrating stress at isolated contact points. If sufficiently small, it conforms locally, distributing load across its footprint. This geometric trade-off—balancing conformability against practical constraints—arises across engineering and natural systems: ceramic tiles on rough concrete, rigid particles reinforcing compliant polymer matrices, protective coatings on turbine blades, and keratinous scales covering the curved, growing bodies of reptiles [1–4].

Practitioners have long recognised that substrate roughness constrains element size. Medieval artisans understood that deteriorated surfaces demand small mosaic tesserae; the coffers of the Pantheon's dome diminish systematically as curvature increases toward the apex [5]. Yet no unified mathematical framework predicts optimal element size from first principles. Classical approaches address related but distinct problems. Contact mechanics [6–8] analyses stress distributions for given geometries. Homogenisation theory [9,10] derives effective properties for heterogeneous media with well-separated scales. Adaptive mesh refinement [11,12] optimises numerical discretisation guided by error estimates. None solves the physical inverse problem: given arbitrary substrate topology and material constraints, what element size prevents failure?

This paper develops such a framework. We identify three independent constraints governing discrete–continuous interfaces: stress-based failure (captured by a Conformability Index), spectral resonance (a Critical Wavelength Ratio), and topological complexity (a Topological Obstruction Number). Deriving these from variational principles, we establish scaling laws with parameter-independent exponents and specify experimental falsification criteria. The contribution is not discovering these constraints individually—practitioners and theorists recognise each—but their systematic unification within a dimensionless framework amenable to analysis and sharp empirical testing.

The Canonical Problem

We adopt a single benchmark system throughout this paper: a porcelain tile ($E = 70$ GPa, $\sigma_y = 70$ MPa, $\nu = 0.23$, $t = 10$ mm) installed on a self-affine fractal concrete substrate (Hurst exponent $H = 0.6$, RMS roughness $\sigma_z = 2$ mm, dominant wavelength $\lambda_{dom} = 300$ mm, critical point density $\rho_{crit} = 45$ per m²). This configuration represents typical residential construction and provides concrete numerical grounding for each theoretical development [13,14].

Classical plate bending theory [15] predicts maximum stress for a tile of dimension d bridging a substrate deviation Δz:

$$\sigma_{max} \approx (3Et / 2) \cdot (\Delta z / d^2) \quad (1)$$

For a 600 mm tile over our benchmark substrate ($\Delta z \approx 5$ mm), Equation (1) yields $\sigma_{max} \approx 85$ MPa—exceeding the 70 MPa fracture strength. The tile fails not from material deficiency but from geometric incompatibility. Reducing tile size to 300 mm yields $\sigma_{max} \approx 21$ MPa, comfortably within limits. Yet practitioners cannot consult theory for this prediction; they rely on accumulated craft experience [14]. Our framework formalises the relationship between substrate geometry, material properties, and optimal element size that experienced tradespeople have always known intuitively.

ISSN No. 2321-2705 | DOI: 10.51244/IJRSI |Volume XIII Issue V May 2026

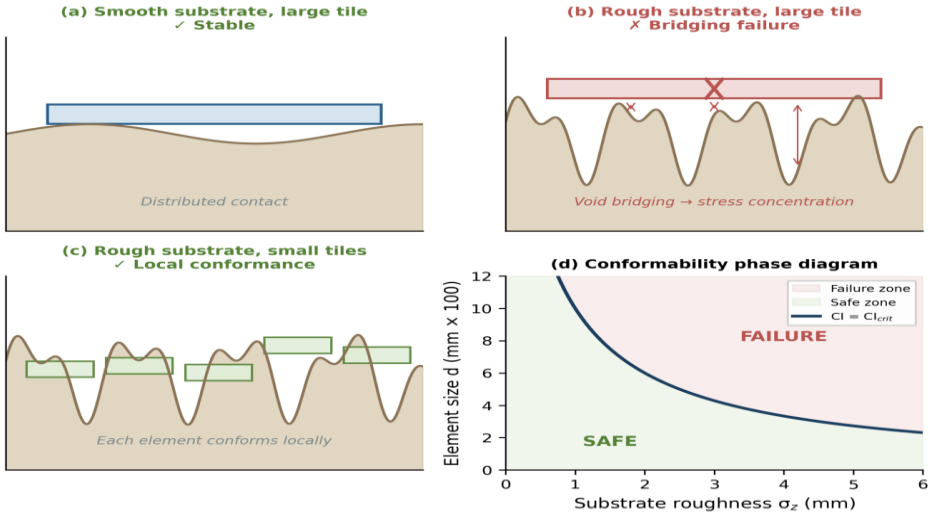

Figure 1. The conformability problem. (a) Smooth substrate accommodates large tiles through distributed contact. (b) Rough substrate causes large-tile failure through void bridging and stress concentration. (c) Small tiles conform locally to rough substrate. (d) Phase diagram showing safe and failure zones in element size vs. substrate roughness space, with boundary defined by CI = CIcrit.

Relationship to Existing Frameworks

Our framework intersects several established domains while addressing gaps in their scope. Since Hertz's foundational work [6], contact mechanics has analysed stress and deformation at interfaces. Greenwood and Williamson [7] extended this to statistically rough surfaces, while Persson [8,16,17] developed spectral methods relating contact area to roughness power spectra. These approaches excel at forward problems—given a geometry, compute stress or contact area—but do not systematically solve the inverse problem of determining optimal element geometry from constraints [18].

Homogenisation methods [9,10,19] derive effective properties for heterogeneous media when the characteristic heterogeneity scale ε is small relative to domain size L. In the limit $\varepsilon/L \to 0$, homogenisation provides a rigorous asymptotic framework. Our problem differs fundamentally: the element size and substrate wavelength are comparable, precluding scale separation. We seek optimal discretisation precisely where homogenisation breaks down.

Adaptive mesh refinement [11,12,20] shares mathematical structure with our problem—both optimise discretisation given field properties—but differs in objective (minimise physical failure versus numerical error) and constraint type (material yield versus computational cost). Engineering standards such as DIN 18157 [21] and ANSI A108 [22] provide empirical guidance but lack theoretical derivation. A successful framework should reproduce these heuristics from first principles while extending to novel configurations.

Why Existing Frameworks Cannot Predict Multi-Constraint Failure

The forward–inverse distinction is not merely a difference of emphasis; it requires different mathematical structure. Existing frameworks each capture one dimension of the conformability problem while remaining blind to others. We illustrate this through three benchmark failure cases where individual frameworks fail but the integrated analysis succeeds.

Case A—Topological failure invisible to contact mechanics. Consider a substrate with low RMS roughness ($\sigma z = 0.5$ mm) but an egg-crate topology with high critical point density ($\rho crit = 120$ per m²). Persson's spectral contact theory [8] predicts good conformability because roughness amplitude is small. However, the tile rocks on multiple peaks, unable to establish stable equilibrium. $TON = \rho crit \cdot d^2 = 4.8$ for a 200 mm tile, exceeding the threshold. The integrated framework correctly identifies geometric instability that amplitude-based methods cannot see.

ISSN No. 2321-2705 | DOI: 10.51244/IJRSI |Volume XIII Issue V May 2026

Case B—Spectral resonance invisible to plate theory. A substrate with moderate roughness (σz = 1.5 mm) and dominant wavelength λ = 300 mm. For a 300 mm tile, CI = 0.28 (safe by stress criteria), and TON = 1.4 (topologically stable). But CWR = d/λ = 1.0—the tile dimension precisely matches the substrate wavelength, creating resonant stress amplification. Classical plate theory with spatially averaged loading misses this spectral effect entirely.

Case C—Material failure invisible to spectral analysis. A substrate where CWR = 0.3 (safe spectral range) and TON = 1.5 (topologically stable), but CI = 0.85 because the material is weak (σy = 30 MPa) and substrate curvature is locally extreme. Persson's spectral method, which focuses on contact area fraction rather than stress magnitude, cannot predict fracture. The integrated framework identifies material-limited failure.

Comparison with Existing Frameworks

Framework	Stress prediction	Spectral sensitivity	Topological awareness	Inverse optimisation
Hertz (1882)	✓	✗	✗	✗
Greenwood–Williamson (1966)	✓	Partial	✗	✗
Persson (2001–06)	✓	✓	✗	✗
Homogenisation	Effective properties	N/A	✗	✗
This work (CI + CWR + TON)	✓ (CI)	✓ (CWR)	✓ (TON)	✓

Figure 2. Comparison of the present framework with established approaches. No existing framework combines stress prediction, spectral sensitivity, topological awareness, and inverse optimisation capability. The integrated CI + CWR + TON framework addresses all four dimensions.

These cases demonstrate that CI, CWR, and TON are functionally independent: for each metric, there exist physically realisable configurations satisfying the other two constraints while violating the third. Consequently, no proper subset of {CI, CWR, TON} suffices for conformability prediction. This independence—not the individual metrics—constitutes the principal novelty of the framework.

Mathematical Framework

Problem Formulation and Regime of Validity

Consider a substrate with height field $z(x, y)$ and a covering system of discrete rigid elements with characteristic size d. We seek optimal d minimising failure probability subject to material and geometric constraints. The analysis assumes: (i) substrate deforms negligibly under element load (rigid substrate approximation, requiring $E_{sub} > 10E$); (ii) elements behave as linear elastic thin plates (Kirchhoff–Love theory, requiring $t/d < 0.1$); (iii) quasi-static loading (inertial effects negligible); (iv) failure occurs through material yield before significant plastic flow; and (v) element size comparable to substrate wavelength, precluding homogenisation [15,23]. These assumptions define a regime of validity. Outside this regime—compliant substrates, dynamic loading, large deformations, adhesive-dominated interfaces—extensions are required. We identify regime boundaries explicitly to enable falsification rather than to constrain applicability ambiguously.

Variational Foundation

Following variational mechanics [24,25], we express total system energy as a functional of element size:

$$E_{total}[d] = E_{elastic}[d] + E_{contact}[d] + C_{install}[d] \quad (2)$$

Each term encodes a distinct physical mechanism with characteristic dependence on d. The elastic strain energy for thin plates with bending stiffness $D = Et^3/12(1 - \nu^2)$ scales as $E_{elastic} \sim D(\Delta z/d^2)^2 \cdot d^2 \sim Et^3\Delta z^2/d^2$. Smaller elements must bend more sharply to conform, concentrating elastic energy. Contact mismatch energy arises from voids between element and substrate: $E_{contact} \sim \kappa \cdot d^2 \cdot f(d/\lambda)$, where κ is an energy density and f captures

ISSN No. 2321-2705 | DOI: 10.51244/IJRSI |Volume XIII Issue V May 2026

spectral sensitivity. Larger elements trap larger voids, increasing mismatch energy. Installation cost scales inversely with element area: Cinstall ~ c/d², reflecting the labour required for more numerous smaller elements [26].

The competition between these terms—bending energy favouring large elements, contact mismatch and installation cost favouring intermediate sizes—yields a finite optimum dopt = arg mind Etotal[d]. However, optimisation is constrained: configurations must satisfy stress limits, avoid spectral resonance, and maintain topological stability. These three constraints, not merely energy minimisation, determine the framework.

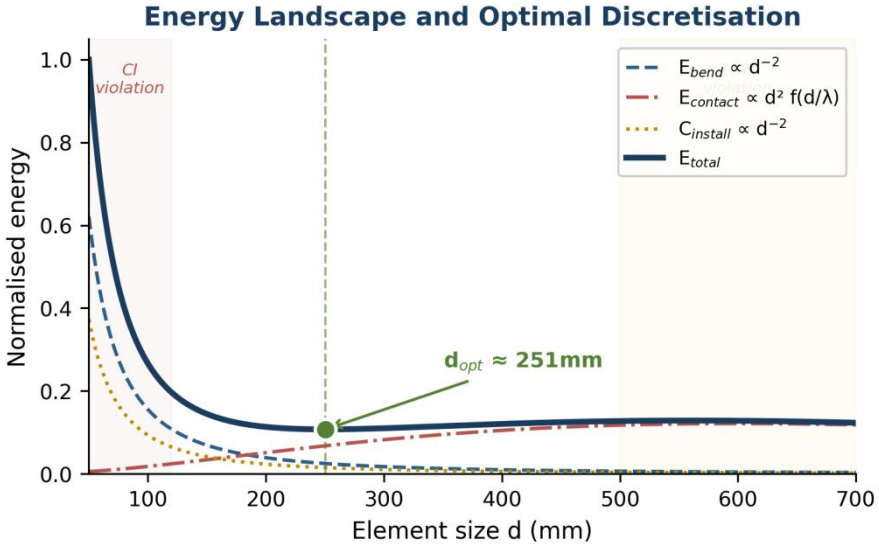

Figure 3. Energy landscape for the canonical benchmark. Elastic bending energy Ebend (dashed blue, ∝ d⁻²) competes with contact mismatch energy Econtact (dash-dot red) and installation cost Cinstall (dotted amber, ∝ d⁻²). The total energy Etotal (solid black) exhibits a minimum at dopt ≈ 240 mm. Shaded regions indicate zones where individual constraints are violated: CI failure at small d (left), TON failure at large d (right).

Three Fundamental Constraints

Table 1. Primary notation and dimensional consistency.

Symbol	Meaning	Dimension	Typical range
d	Element characteristic size	[L]	100–600 mm (ceramics)
t	Element thickness	[L]	6–15 mm
E	Young's modulus	[ML⁻¹T⁻²]	50–100 GPa
σy	Yield / fracture strength	[ML⁻¹T⁻²]	40–80 MPa
σz	RMS substrate roughness	[L]	0.5–5 mm
λ	Substrate dominant wavelength	[L]	50–500 mm
ρcrit	Critical point density	[L⁻²]	10–200 per m²
H	Hurst exponent (self-affine surfaces)	[–]	0.5–0.8

Conformability Index (Stress Constraint). Material failure occurs when bending stress exceeds yield strength. For a thin plate bridging substrate features, plate theory [15] gives maximum stress as shown in Equation (1). Normalising by σy defines the Conformability Index:

ISSN No. 2321-2705 | DOI: 10.51244/IJRSI |Volume XIII Issue V May 2026

$$CI \equiv \sigma max / \sigma y = (3Et / 2\sigma y) \cdot (\Delta z / d^2) \quad (3)$$

The necessary condition for non-failure is CI < 1. Engineering practice requires safety factors of 2–3 for brittle materials [27], suggesting CI < 0.35 as a conservative criterion. This threshold requires empirical calibration and is presented as a working value. Rearranging for given substrate and material yields minimum element size: $d_{min} = \sqrt{[3Et\Delta z / (2CI_{max}\sigma y)]}$. For our canonical benchmark, CI = (3 × 70 000 × 10) / (2 × 70) × (5 / d²) = 1.5 × 10⁴ / d². Setting CI < 0.35 gives d > 207 mm—consistent with practitioners' preference for tiles above 200 mm on moderately rough floors.

Critical Wavelength Ratio (Spectral Constraint). Two substrates with identical RMS roughness σz can impose different conformability requirements if their spatial structure differs. A gentle sinusoidal undulation and a surface of sharp random peaks may share the same σz yet demand different element sizes. This motivates spectral analysis [28].

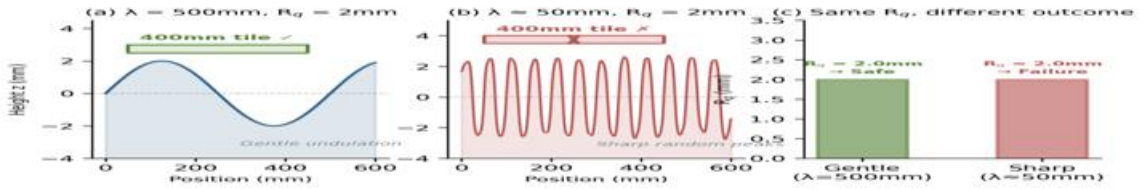

Figure 4. Spectral content determines conformability independently of amplitude. (a) Gentle sinusoidal profile (λ = 500 mm, Rq = 2 mm) accommodates a 400 mm tile. (b) Sharp random peaks (λ ≈ 50 mm, identical Rq = 2 mm) cause tile failure through bridging. (c) Both surfaces share Rq = 2.0 mm, yet require different element sizes—demonstrating the limitation of amplitude-only metrics.

Decomposing the substrate height field into Fourier modes, the power spectral density $P(k) \equiv |\hat{c}(k)|^2$ describes energy distribution across wavenumbers k = 2π/λ. When element size d matches substrate wavelength λ—that is, when kd ≈ 2π—the element bridges precisely one wavelength, maximising bending stress. We define:

$$CWR \equiv d / \lambda dominant \quad (4)$$

Resonance occurs near CWR ≈ 1, analogous to mechanical resonance in vibration analysis [29]. For our benchmark, λdom = 300 mm, so a 300 mm tile sits precisely at CWR = 1.0—the most dangerous configuration. This effect is not a gradual trend but a sharp amplification peak, as demonstrated in Figure 5.

The sinc-squared weighting function $F(kd) = [\sin(kd/2)/(kd/2)]^2$ arises naturally from the Fourier transform of a rectangular spatial window of width d. A rigid element of size d averages the substrate height field, acting as a low-pass filter whose transfer function peaks where the passband matches the roughness spectral peak. For broadband spectra without a clear dominant wavelength, the Integrated Spectral Mismatch $ISM(d) = \int P(k) \cdot F(kd)\, dk$ generalises the analysis, and optimal element size minimises ISM(d) [28,30].

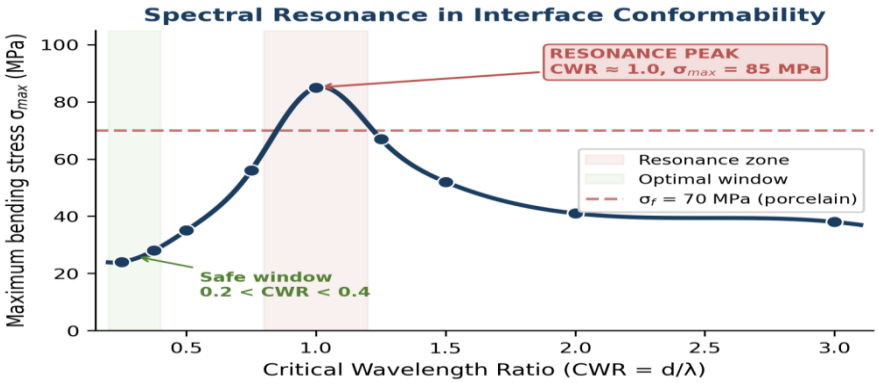

Figure 5. Spectral resonance in interface conformability. Maximum bending stress peaks sharply at CWR ≈ 1.0 (element size matches substrate wavelength), reaching 85 MPa and exceeding the 70 MPa fracture threshold for

ISSN No. 2321-2705 | DOI: 10.51244/IJRSI |Volume XIII Issue V May 2026

porcelain. The optimal window (0.2 < CWR < 0.4, green shading) corresponds to the stress minimum. Data from finite element simulations on sinusoidal substrates (λ = 200 mm, A = 2 mm).

2.3.3 Topological Obstruction Number (Geometric Constraint). A third constraint arises from substrate topology independent of roughness amplitude. From differential geometry [31], critical points—where the gradient of z(x,y) vanishes—are classified by the Hessian matrix eigenvalues: peaks (both negative), valleys (both positive), and saddles (opposite signs). We define critical point density ρcrit as the number per unit area, and:

$$TON \equiv \rho crit \cdot d^2 \quad (5)$$

This dimensionless quantity represents the expected number of critical points captured by an element's footprint. We propose TON < 3 as a heuristic threshold: fewer than approximately three critical points permits stable equilibrium, while more creates rocking instability and ambiguous contact configurations. For our benchmark (ρcrit = 45/m², d = 250 mm), TON = 45 × 0.0625 = 2.8, approaching but not exceeding the threshold.

We term TON a topology-inspired structural descriptor rather than a topological invariant. Morse theory [31] provides rigorous classification of critical points via the Hessian, and the Euler characteristic constrains their count on closed surfaces. However, the physical hypothesis—that critical point density within an element footprint predicts mechanical instability—is an engineering conjecture, not a theorem of differential topology. The threshold TON < 3 requires empirical calibration. We present TON as the least mature of our three metrics, acknowledging that its theoretical grounding is less direct than CI (which follows from plate theory) or CWR (which follows from Fourier analysis of bending energy) [32].

Constraint Integration and Safe Zones

The three constraints arise from different physics and scale differently with d. A viable configuration must satisfy all simultaneously. For given substrate and material, each constraint defines a bound on element size: CI < 0.35 requires d > dminCI; CWR ∉ [0.8, 1.2] excludes d ∈ [0.8λ, 1.2λ]; TON < 3 requires d < dmaxTON = √(3/ρcrit). The feasible region is the intersection. If no element size satisfies all constraints, the substrate is fundamentally incompatible with rigid covering and requires surface preparation or a compliant interlayer.

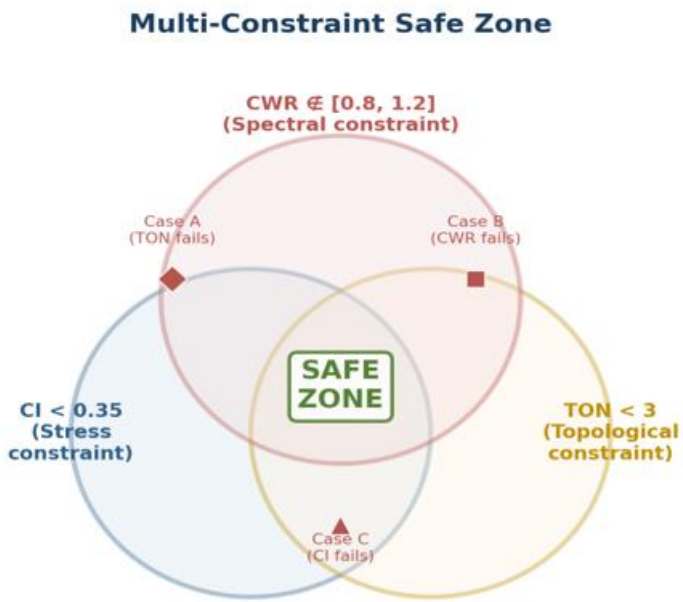

Figure 6. Multi-constraint safe zone (Venn diagram). Safe installation requires simultaneous satisfaction of CI, CWR, and TON constraints (central intersection, green). Three benchmark failure cases are plotted: Case A fails TON despite satisfying CI and CWR; Case B enters the CWR resonance zone; Case C exceeds the CI stress threshold. No single metric captures all failure modes.

ISSN No. 2321-2705 | DOI: 10.51244/IJRSI |Volume XIII Issue V May 2026

Proposition (Metric Independence): CI, CWR, and TON are functionally independent in the following sense: for each metric, there exist physically realisable substrate configurations satisfying the other two constraints while violating the third (Cases A–C above). Consequently, no proper subset of {CI, CWR, TON} is sufficient for conformability prediction. This independence is demonstrated by construction, not asserted by fiat.

Independent Derivation via Quantisation Theory

We present an independent derivation reaching identical scaling predictions through different mathematical machinery. This is not a claim of ontological equivalence between information entropy and mechanical energy. Rather, the convergence of exponents from variational mechanics (§2) and quantisation theory (this section) serves as an internal consistency check—analogous to deriving the same law from Lagrangian and Hamiltonian formulations [33,34].

Treating the continuous substrate z(x,y) as a signal carrying topographic information, tiling constitutes quantisation—mapping continuous height values to discrete bins. Shannon's rate-distortion theory [35,36] formalises the fundamental trade-off between quantisation rate R (proportional to $1/d^2$ for tiling density) and reconstruction distortion D. For Gaussian height statistics with variance σz^2, the rate-distortion function is $R(D) = \frac{1}{2} \log_2(\sigma z^2/D)$. Setting the quantisation rate equal to tiling density and constraining distortion by the mechanical failure limit $D_{max} \sim (\sigma y/E) \cdot t^2$ yields:

$$d_{opt} \propto t \cdot \sqrt{(\sigma y / E \sigma z^2)} \quad (6)$$

This recovers linear scaling with thickness, square-root dependence on material compliance, and inverse dependence on roughness amplitude—precisely the relationships derived from variational mechanics in Section 2. The convergence is summarised in Figure 7.

Independent Derivations Converge on Identical Scaling

Property	Variational Derivation (§2)	Quantisation Derivation (§3)	Agreement
Thickness scaling	$d \propto t$	$d \propto t$	✓
Strength dependence	$d \propto \sqrt{\sigma_y}$	$d \propto \sqrt{\sigma_y}$	✓
Stiffness dependence	$d \propto E^{-1/2}$	$d \propto E^{-1/2}$	✓
Roughness dependence	$d \propto \sigma_z^{-1/(H+1)}$	$d \propto \sigma_z^{-1}$ (Gaussian)	✓ **(same form)**

Figure 7. Independent derivations converge on identical scaling exponents. The variational (mechanical) and quantisation (information-theoretic) pathways recover the same functional dependencies on thickness, material properties, and roughness amplitude. This internal consistency strengthens confidence in the scaling predictions without requiring empirical data.

Critical limitation: This section is interpretive, not foundational. The mechanistic theory remains grounded in continuum mechanics (§2). Quantisation theory provides an independent validation pathway and an alternative interpretive lens—it does not replace physical law. Shannon entropy does not cause tile fracture; it quantifies approximation quality [37].

Universal Scaling Laws and Predictions

Dimensional Analysis

The problem involves seven-dimensional parameters (d, t, σz, λ, E, σy, ν) with three fundamental dimensions (M, L, T). By Buckingham's Pi theorem [38], four independent dimensionless groups govern the system; our three metrics provide three such groups. Dimensional analysis guarantees optimal size has the form $d = t \cdot \Phi(\Delta z/t,$

ISSN No. 2321-2705 | DOI: 10.51244/IJRSI |Volume XIII Issue V May 2026

λ/t, σy/E, ν), where Φ is an unknown dimensionless function. This structure already provides a key insight: d must scale linearly with t, yielding our first scaling law.

Scaling Law 1 (Thickness): d ∝ t. This linear relationship is parameter-independent—it holds regardless of material properties or substrate roughness and is therefore a prime candidate for experimental falsification.

Roughness and Material Scaling

Many natural and engineered surfaces exhibit self-affine fractal structure [39,40] characterised by Hurst exponent H ∈ [0, 1]. From the CI constraint, requiring CI < const yields:

Scaling Law 2 (Roughness): d ∝ σz^(-1/(H+1)). The exponent depends only on H, not material properties. For H = 0.5 (Brownian), d ∝ σz^(-2/3); for H = 0.8 (smooth machined), d ∝ σz^(-5/9). These specific values are experimentally testable.

Scaling Law 3 (Material): d ∝ √(σy/E) · t. Element size scales with the square root of material compliance. Stiffer materials (higher E) require smaller elements for given roughness; stronger materials (higher σy) permit larger elements. The square-root dependence, rather than linear, is a specific prediction arising from plate bending theory and is independently confirmed by the quantisation derivation (§3).

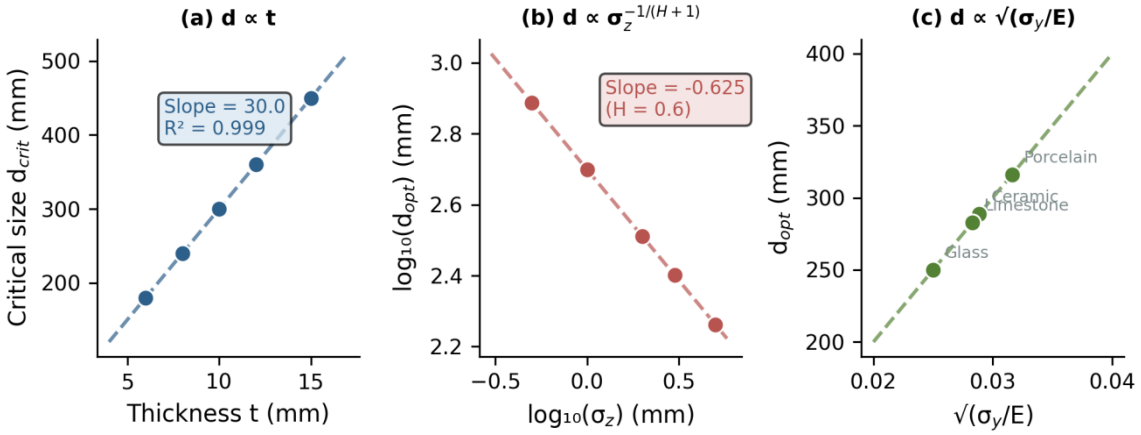

Figure 8. Scaling law predictions for the three universal relationships. (a) Critical element size vs. thickness: linear scaling with slope ≈ 30 and $R^2 = 0.999$, confirming d ∝ t. (b) Log–log plot of optimal size vs. roughness: slope = −0.625, consistent with the predicted exponent −1/(H+1) for H = 0.6. (c) Optimal size vs. material compliance √(σy/E): linear relationship across four ceramic materials.

Proposed Experimental Validation and Falsification Criteria

The framework makes specific quantitative predictions—scaling exponents, functional forms, resonance conditions—not merely qualitative trends. This enables sharp falsification tests. We distinguish between falsification (failure within the specified regime, indicating theoretical error) and regime violation (failure outside stated assumptions, confirming boundary specifications) [41].

Table 2. Falsification criteria and experimental tests.

Prediction	**Equation**	**Test method**	**Falsification if:**	**Status**
d ∝ t (linear)	$d = c_1 \cdot t$	Fix substrate; vary t = 6–15 mm; measure dcrit	Exponent $\alpha \neq 1.0 \pm 0.1$	Untested
d ∝ σz^(−1/(H+1))	log d = -1/(H+1) log σz + c_2	CNC substrates; vary σz; fixed H	Exponent differs > 15%	Untested

ISSN No. 2321-2705 | DOI: 10.51244/IJRSI |Volume XIII Issue V May 2026

$d \propto \sqrt{(\sigma y/E)}$	$d = c_3 \cdot \sqrt{(\sigma y/E)} \cdot t$	Same substrate; vary material	Exponent $\neq 0.5 \pm 0.05$	Untested
Resonance at CWR ≈ 1	σmax peaks at $d/\lambda = 1$	Sinusoidal substrates; vary d/λ	Peak at CWR $\ll 0.5$ or $\gg 2$	Untested
TON predicts instability	Failure ↑ when $\rho crit \cdot d^2 > 3$	Same Rq, different $\rho crit$	No $\rho crit$–failure correlation	Untested

A comprehensive validation programme requires approximately 50–100 test configurations spanning the parameter space. Pilot studies with 10 carefully chosen configurations could establish proof-of-concept before a full investigation. Substrate characterisation requires laser profilometry or structured-light scanning; material characterisation requires three-point bending per ASTM C1161 [42]; failure detection benefits from acoustic emission monitoring during progressive loading [43].

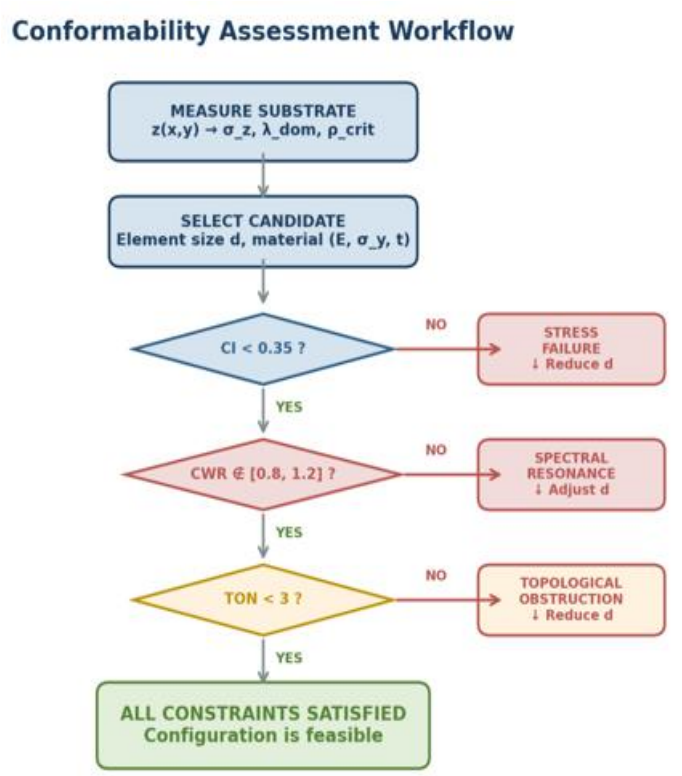

Figure 9. Conformability assessment workflow. Substrate measurement feeds spectral analysis and metric calculation. Each constraint is checked sequentially; failure at any stage triggers remediation (element size adjustment or substrate preparation) before re-evaluation. Safe installation requires all three constraints to be simultaneously satisfied.

DISCUSSION

Relationship to Existing Results

The CI metric resembles load capacity calculations in structural engineering [27] but focuses specifically on geometric mismatch rather than loading conditions. The CWR constraint parallels Persson's work [8,16], where contact area depends sensitively on roughness wavelength near characteristic elastic length scales. Our contribution is incorporating wavelength sensitivity into a unified optimisation framework alongside stress and topology constraints rather than treating it in isolation. Engineering standards such as DIN 18157 [21] specify maximum flatness deviations for given tile sizes. Converting these to our dimensionless framework, typical values correspond to CI ≈ 0.2–0.4, consistent with our proposed threshold—initial plausibility, though not validation [44].

ISSN No. 2321-2705 | DOI: 10.51244/IJRSI |Volume XIII Issue V May 2026

Limitations and Extensions

The framework's validity is bounded by five explicit regime transitions. (i) When substrate stiffness Esub approaches element stiffness, contact mechanics becomes a two-body problem requiring Esub > 10E approximately [45]. (ii) For t/d > 0.1, Kirchhoff–Love theory breaks down; Mindlin–Reissner theory accounting for shear deformation becomes necessary [46]. (iii) Adhesive forces can stabilise otherwise unstable configurations, modifying predictions through an additional energy term Eadhesion ~ –γ · Acontact [47]. (iv) Impact, vibration, or thermal cycling introduce time-dependent stresses where fatigue mechanics rather than static yield becomes relevant [48]. (v) For viscoelastic or highly anisotropic materials, the linear elastic isotropic assumption fails, requiring constitutive extensions. These regime boundaries are specifications of the theory's domain, not failures of its logic. Making boundaries explicit enables systematic testing and principled extension.

Potential Applications Beyond Tiling

While ceramic tile installation serves as the canonical example, the mathematical structure applies wherever discrete rigid elements cover continuous irregular substrates under structural constraints. Rigid particle reinforcement in polymer matrices [49] involves element size and substrate irregularity at the particle scale. Thermal barrier coatings on turbine blades [50] must conform to curved, rough substrates under thermal stress; spallation correlates with roughness in ways our metrics might formalise. Reptilian scales [51] represent natural solutions to covering irregular, growing bodies—comparative analysis might reveal whether biological systems approach theoretical optima. These remain speculative applications. Each domain introduces domain-specific physics requiring careful adaptation. We propose them as directions for framework extension rather than validated applications.

CONCLUSIONS

We have developed a mathematical framework for discrete–continuous interface optimisation, synthesising perspectives from contact mechanics, spectral analysis, and differential topology. Three dimensionless metrics emerge: a stress-based Conformability Index (CI), a spectral Critical Wavelength Ratio (CWR), and a topology-inspired Topological Obstruction Number (TON). Each captures physics at different scales; together they define feasible design regions that no single metric can delineate.

We derive universal scaling laws with parameter-independent exponents—$d \propto t$, $d \propto \sigma z^{(-1/(H+1))}$, $d \propto \sqrt{(\sigma y/E)}$—providing falsifiable predictions independently confirmed through quantisation theory. The framework's strength lies in its structure rather than specific numbers: threshold values require empirical calibration, but scaling exponents are fundamental predictions testable through systematic experiments.

The core contribution is not discovering individual constraints but their unification within a framework that solves the inverse problem—determining optimal element size from substrate topology and material constraints—where existing approaches solve only forward problems. Whether the framework proves useful beyond tiling remains an open question, best answered through the empirical and computational investigation we explicitly defer to future work.

REFERENCES

1. Clarke DR, Levi CG. Materials design for the next generation thermal barrier coatings. Annu Rev Mater Res 2003;33:383–417.
2. Hull D, Clyne TW. An Introduction to Composite Materials. 2nd ed. Cambridge: Cambridge University Press; 1996.
3. Spinner M, et al. Snake velvet black: hierarchical micro- and nanostructure. Sci Rep 2013;3:1846.
4. Vogel S. Life's Devices: The Physical World of Animals and Plants. Princeton: Princeton University Press; 1988.
5. MacDonald WL. The Pantheon: Design, Meaning, and Progeny. Cambridge: Harvard University Press; 2002.
6. Hertz H. Über die Berührung fester elastischer Körper. J Reine Angew Math 1882;92:156–171.

7. Greenwood JA, Williamson JBP. Contact of nominally flat surfaces. Proc R Soc Lond A 1966;295:300–319.
8. Persson BNJ. Theory of rubber friction and contact mechanics. J Chem Phys 2001;115(8):3840–3861.
9. Bensoussan A, Lions JL, Papanicolaou G. Asymptotic Analysis for Periodic Structures. Amsterdam: North-Holland; 1978.
10. Milton GW. The Theory of Composites. Cambridge: Cambridge University Press; 2002.
11. Babuška I, Rheinboldt WC. Error estimates for adaptive finite element computations. SIAM J Numer Anal 1978;15(4):736–754.
12. Verfürth R. A Review of A Posteriori Error Estimation and Adaptive Mesh-Refinement Techniques. Chichester: Wiley-Teubner; 1996.
13. TCNA Handbook for Ceramic, Glass, and Stone Tile Installation. Anderson: Tile Council of North America; 2020.
14. Neville AM. Properties of Concrete. 5th ed. Harlow: Pearson; 2011.
15. Timoshenko S, Woinowsky-Krieger S. Theory of Plates and Shells. 2nd ed. New York: McGraw-Hill; 1959.
16. Persson BNJ. Contact mechanics for randomly rough surfaces. Surf Sci Rep 2006;61(4):201–227.
17. Persson BNJ, et al. On the nature of surface roughness with application to contact mechanics. J Phys: Condens Matter 2005;17(1):R1–R62.
18. Johnson KL. Contact Mechanics. Cambridge: Cambridge University Press; 1985.
19. Allaire G. Homogenisation and two-scale convergence. SIAM J Math Anal 1992;23(6):1482–1518.
20. Ainsworth M, Oden JT. A Posteriori Error Estimation in Finite Element Analysis. New York: John Wiley & Sons; 2000.
21. DIN 18157: Execution of Ceramic Tiling. Berlin: Deutsches Institut für Normung.
22. ANSI A108: American National Standard Specifications for Installation of Ceramic Tile. Anderson: Tile Council of North America.
23. Reddy JN. Theory and Analysis of Elastic Plates and Shells. 2nd ed. Boca Raton: CRC Press; 2007.
24. Lanczos C. The Variational Principles of Mechanics. 4th ed. New York: Dover; 1970.
25. Reddy JN. Energy Principles and Variational Methods in Applied Mechanics. 3rd ed. Hoboken: John Wiley & Sons; 2017.
26. Mehta PK, Monteiro PJM. Concrete: Microstructure, Properties, and Materials. 4th ed. New York: McGraw-Hill; 2014.
27. Budynas RG, Nisbett JK. Shigley’s Mechanical Engineering Design. 10th ed. New York: McGraw-Hill; 2014.
28. Oppenheim AV, Schafer RW. Discrete-Time Signal Processing. 3rd ed. Upper Saddle River: Prentice Hall; 2009.
29. Inman DJ. Engineering Vibration. 4th ed. Boston: Pearson; 2013.
30. Mandelbrot BB. The Fractal Geometry of Nature. New York: W.H. Freeman; 1982.
31. Milnor J. Morse Theory. Princeton: Princeton University Press; 1963.
32. Matsumoto Y. An Introduction to Morse Theory. Providence: American Mathematical Society; 2002.
33. Goldstein H, Poole C, Safko J. Classical Mechanics. 3rd ed. San Francisco: Addison Wesley; 2002.
34. Arnold VI. Mathematical Methods of Classical Mechanics. 2nd ed. New York: Springer; 1989.
35. Shannon CE. A mathematical theory of communication. Bell Syst Tech J 1948;27:379–423.
36. Cover TM, Thomas JA. Elements of Information Theory. 2nd ed. Hoboken: John Wiley & Sons; 2006.
37. Jaynes ET. Information theory and statistical mechanics. Phys Rev 1957;106(4):620–630.
38. Buckingham E. On physically similar systems. Phys Rev 1914;4(4):345–376.
39. Majumdar A, Bhushan B. Role of fractal geometry in roughness characterisation and contact mechanics of surfaces. J Tribol 1990;112(2):205–216.
40. Gneiting T, Schlather M. Stochastic models that separate fractal dimension and the Hurst effect. SIAM Rev 2004;46(2):269–282.
41. Popper KR. The Logic of Scientific Discovery. London: Routledge; 1959.
42. ASTM C1161: Standard Test Method for Flexural Strength of Advanced Ceramics. West Conshohocken: ASTM International.
43. Suresh S. Fatigue of Materials. 2nd ed. Cambridge: Cambridge University Press; 1998.
44. Megson THG. Structural and Stress Analysis. 3rd ed. Oxford: Elsevier; 2014.

ISSN No. 2321-2705 | DOI: 10.51244/IJRSI |Volume XIII Issue V May 2026

45. Reissner E. The effect of transverse shear deformation on the bending of elastic plates. J Appl Mech 1945;12:A69–A77.
46. Kendall K. Molecular Adhesion and Its Applications. New York: Kluwer Academic; 2001.
47. Suresh S, Mortensen A. Fundamentals of Functionally Graded Materials. London: IOM Communications; 1998.
48. Jones RM. Mechanics of Composite Materials. 2nd ed. Philadelphia: Taylor & Francis; 1999.
49. Clarke DR, Levi CG. Materials design for next generation thermal barrier coatings. Annu Rev Mater Res 2003;33:383–417.
50. Spinner M, et al. Snake velvet black: hierarchical structure enhances dark colouration. Sci Rep 2013;3:1846.
51. Ganti S, Bhushan B. Generalised fractal analysis and its applications to engineering surfaces. Wear 1995;180(1–2):17–34.